Published in final edited form as:
Neuron. 2010 March 25; 65(6): 912–926. doi:10.1016/j.neuron.2010.02.011.

Odor Information Processing by the Olfactory Bulb Analyzed in Gene-Targeted Mice

Jie Tan[1,2], **Agnès Savigner**[3], **Minghong Ma**[3], and **Minmin Luo**[2,4,*]

[1]Institute of Biophysics, Chinese Academy of Sciences, Beijing 100101, China

[2]National Institute of Biological Sciences, Beijing 102206, China

[3]Department of Neuroscience, University of Pennsylvania School of Medicine, Philadelphia, PA 19104, USA

[4]School of Life Sciences, Tsinghua University, Beijing 100084, China

SUMMARY

In mammals, olfactory sensory neurons (OSNs) expressing a specific odorant receptor (OR) gene project with precise stereotypy onto mitral/tufted (M/T) cells in the main olfactory bulb (MOB). It remains challenging to understand how incoming olfactory signals are transformed into outputs of M/T cells. By recording from OSNs expressing mouse I7 receptor and their postsynaptic neurons in the bulb, we found that I7 OSNs and their corresponding M/T cells exhibit similarly selective tuning profiles at low concentrations. Increasing the concentration significantly reduces response selectivity for both OSNs and M/T cells, although the tuning curve of M/T cells remains comparatively narrow. By contrast, interneurons in the MOB are broadly tuned, and blocking GABAergic neurotransmission reduces selectivity of M/T cells at high odorant concentrations. Our results indicate that olfactory information carried by an OR is channeled to its corresponding M/T cells and support the role of lateral inhibition via interneurons in sharpening the tuning of M/T cells.

INTRODUCTION

The mammalian olfactory system can detect a large number of volatile chemicals with vastly diverse molecular structures and discriminate odorants with subtle structural differences. At the level of the peripheral nervous system, this feat is accomplished by millions of OSNs expressing over 1000 OR genes (Buck and Axel, 1991; Zhang et al., 2007). Each OSN in the main olfactory epithelium (MOE) expresses one OR gene, and OSNs expressing a common OR project their axons to one or a few topographically stereotypical loci (glomeruli) out of a total of ~1800 in the MOB (Mombaerts et al., 1996; Ressler et al., 1994; Vassar et al., 1994). This precise projection thus forms an intricate two-dimensional olfactory map in the bulb. A given OR can be activated by a few odorants, and an odorant at behaviorally relevant concentrations activates a sparse set of glomeruli, suggesting that olfactory information is encoded by combinatorial patterns of glomerular activation (Malnic et al., 1999; Rubin and Katz, 1999; Soucy et al., 2009; Uchida et al., 2000; Wachowiak and Cohen, 2001).

*Correspondence: luominmin@nibs.ac.cn.

SUPPLEMENTAL INFORMATION Supplemental Information includes five figures and two tables and can be found with this article online at doi:10.1016/j.neuron.2010.02.011.

How are the incoming signals carried by OSNs translated to the output of the MOB? Within each glomerulus, a few thousand OSNs converge to provide excitatory inputs to 25–50 M/T cells, the bulbar projection neurons (Shepherd et al., 2004). Each M/T cell receives its primary excitatory input from OSNs by extending a single primary dendrite into only one glomerulus. M/T cells also interact extensively through their lateral connections with primarily γ-aminobutyric acid (GABA)-ergic inhibitory interneurons, including periglomerular (PG) cells in the glomerular layer and granule cells in the granule cell layer. Physiological recordings suggest that these inhibitory connections may provide a mechanism of lateral inhibition (Chen et al., 2000; Isaacson and Strowbridge, 1998; Schoppa et al., 1998; Yokoi et al., 1995). It has been hypothesized that the tuning of a M/T cell reflects that of its presynaptic OSNs and is further sharpened by the intrabulbar neuronal circuit (Mori et al., 1999). Although studies in recent decades have contributed substantially to our understanding of odor representation by neurons in the MOB, no studies have directly shown that a M/T cell responds selectively to the odorant ligands of its corresponding OR. In addition, the exact role of lateral inhibition in shaping the odor representation in M/T cells is controversial (Fantana et al., 2008; Laurent, 1999; Wilson and Mainen, 2006). In fact, odor representation appears to be broadened in the fish olfactory bulb (Friedrich and Laurent, 2001) and in the insect antennal lobe (AL) (Schlief and Wilson, 2007; Bhandawat et al., 2007; Wilson et al., 2004). Because these two structures are believed to possess circuitry analogous to that of the mammalian MOB, it remains unclear whether odor representation is similarly broadened at the level of M/T cell output in mammals.

The key to understanding the functional role of the MOB is to compare the odor representations of OSNs and those of their postsynaptic projection neurons. This comparison in the *Drosophila* olfactory system has generated valuable insights into our understanding of the olfactory coding scheme in insects (Schlief and Wilson, 2007; Bhandawat et al., 2007; Wilson et al., 2004). However, it had been technically challenging to perform similar analyses in mammals. The mammalian MOB has a much greater number of glomeruli (~1800 in mice versus ~50 in *Drosophila*) and larger size (a glomerulus in mice has roughly the size of the entire *Drosophila* AL), hindering targeted recordings from M/T cells associated with a specific OR. Physiological studies so far have mostly been performed by randomly recording the olfactory responses from the bulbar neurons without knowing the response profiles of their presynaptic OSNs.

To overcome these difficulties, we analyzed the olfactory response profiles of OSNs expressing mouse I7 receptor and those of their postsynaptic M/T cells from mI7→M71-GFP mice. In these mice, the mouse *I7* gene is swapped into the *M71* receptor locus, and green fluorescent protein (GFP) is expressed in mI7→M71 OSNs (simplified as I7 OSNs below) (Bozza et al., 2002). The ligands for the I7 receptor have been explored in previous studies (Araneda et al., 2000; Bozza et al., 2002; Krautwurst et al., 1998; Zhao et al., 1998), allowing us to systematically characterize the response profiles of I7 OSNs at different odorant concentrations. In addition, these GFP^+ OSNs form normal glomeruli and instruct functional circuitry in the dorsal MOB (Belluscio et al., 2002; Bozza et al., 2002), thus allowing us to record from the M/T cells receiving direct input from these OSNs. Direct comparison of the response profiles of the M/T cells and OSNs corresponding to the same OR enables us to test whether the odor representation of each processing channel is sharpened or broadened in the MOB. To investigate the role of the intrabulbar circuitry in shaping odor representation, we further examined the response profiles of interneurons and the effects of blocking GABAergic synaptic transmission on the responses of I7 M/T cells.

RESULTS

The Response Sensitivity and Selectivity of I7 OSNs

One of the key advantages of using mI7→M71-GFP mice is that I7 is the best-characterized OR. Rat I7 receptor can be strongly activated by octanal (Araneda et al., 2000; Bozza et al., 2002; Zhao et al., 1998), although it also responds to a series of aldehydes with less sensitivity (Araneda et al., 2000; Bozza et al., 2002). Ca^{2+} imaging in cells transfected with the mouse I7 receptor gene shows that the mouse I7 receptor is activated selectively by heptanal but not by octanal and many other odorants at a concentration of 10 μM(Krautwurst et al., 1998). Ca^{2+} imaging in the dissociated OSNs from mI7→M71-GFP mice reveals that I7 OSNs are strongly activated by heptanal and several other aldehydes at 25 μM (Bozza et al., 2002). Based on these findings, we first sought to examine the response sensitivity of I7 OSNs by directly recording the neuronal firing of action potentials from the olfactory epithelium of mI7→M71-GFP mice.

Using the cell-attached patch approach, we recorded odorant-evoked firing of action potentials from individual dendritic knobs of OSNs (Figure 1A). I7 OSNs were identified by strong green fluorescence in the knob and cilia in a preparation that largely maintained the integrity of the MOE (Figure 1B) (Grosmaitre et al., 2006). Odorants at different concentrations were delivered by pressure ejection through a seven-barrel pipette. All I7 OSNs tested were activated by heptanal at concentrations as low as 1 μM, with saturation at ~100 μM (Figures 1C and 1E). Consistent with previous studies on odorant-evoked responses in OSNs (Duchamp-Viret et al., 1999), heptanal at higher concentrations typically elicited responses consisting of an initial increase in firing that was followed by a period of silence and a secondary increase in firing (Figure 1C). Based on an established protocol of analyzing OSN responses (Rospars et al., 2003), we defined the odor-evoked responses as the median instantaneous firing frequency immediately after odorant application. We summarize the dose-response relationship from 10 I7 OSNs in Figure 1E. For each neuron, the odor-evoked responses at different concentrations were normalized to the saturating response. The data at each concentration were then averaged and fit with a sigmoid function, which reported the half-maximal effective concentration (EC_{50}) for heptanal as −5.20 ± 0.14 log molar concentration (~6.3 μM; mean ± SEM; Figure 1F).

I7 OSNs responded to octanal with lower sensitivity (Figures 1D and 1E). Most of these cells were activated by octanal only at concentrations ≥10 μM. Octanal responses saturated at 1 mM, and the maximal response to octanal was only ~85% of that to heptanal (Figure 1E). The EC_{50} for octanal (−4.2 ± 0.2 log molar or ~63.1 μM; n = 10) was significantly higher than that for heptanal (Figure 1F), indicating that I7 OSNs respond to heptanal with ~10 times higher sensitivity than is observed in the response to octanal.

We next examined the selectivity of I7 OSNs to various odorants at different concentrations. OSNs expressing rat I7 respond strongly to a subset of aldehydes but not to molecules of other functional groups, such as acetate, ketone, and acid (Araneda et al., 2000). Because of the limit of our odor-delivery system, we chose to test the response selectivity to a set of six aldehydes, several of which activate I7 OSNs at a relatively high concentration (Bozza et al., 2002). At the concentration of 1 μM, heptanal but none of the other five aldehydes evoked clear responses (Figures 2A and 2B). By contrast, four of these aldehydes at the concentration of 10 μM induced increases in the firing frequency from I7 OSNs (Figures 2C and 2D). As expected, the response profile of I7 OSNs broadens when stimulated by odorants at higher concentrations.

The Response Sensitivity of I7 M/T Cells

Following characterization of the response sensitivity and selectivity of I7 OSNs, we examined the response properties of their postsynaptic M/T cells from anesthetized, freely breathing

mI7→M71-GFP mice. The GFP-labeled glomeruli were located on the dorsal MOB in a bilaterally symmetric manner (Figure S1A). Because the primary dendrites of M/T cells express active conductance and their spiking activity accurately reflects the output of these cells (Chen et al., 1997, 2002; Shen et al., 1999), recording electrodes were targeted to the primary dendritic trunks of M/T cells within the GFP glomeruli under the guidance of two-photon microscopy (Figures 3A–3C). Odorants were initially diluted in mineral oil, and saturated odor vapor was further diluted and applied by injection into the continuous airstream (Figure 3B). After recordings, neurons were juxtacellularly labeled to determine their morphological cell types (Figure 3D). Their association with I7 glomeruli was identified by examining whether their primary dendritic tufts were located in the GFP-labeled glomeruli.

Heptanal elicited vigorous firing of action potentials from all I7 M/T cells of different subtypes, including mitral (Figure 3E; n = 7 cells), middle tufted (Figure 3F; n = 26 cells), and external tufted cells (Figure 3G; n = 7 cells; mean response strength for all I7 M/T cells = 16.0 ± 1.7 spikes/s at 1% dilution). Odorant responses were recorded reliably from trial to trial (Figure S1B). Responses typically started at ~300 ms after valve opening and ended soon after pulse termination (Figures 3E–3G). Odor-evoked firing of action potentials was usually coupled to respiratory rhythm, with most of the responses occurring during a specific phase of the respiratory cycles (Figure S1C–S1E). We observed similar response strengths in mitral, middle tufted, and external tufted cells to heptanal at both 0.1% and 1% dilutions (Figure S1F). So in the following experiments, we combined data from the three subtypes of I7 projection neurons to report them as a single group.

Because I7 OSNs respond to heptanal and octanal with different sensitivity, we tested how I7 M/T cells responded to these two odorants at a series of concentrations. For the purpose of comparing the sensitivity of I7 M/T cells and that of I7 OSNs, we converted the concentration of heptanal and octanal from vapor dilution to molar concentration. Clear excitatory response was evoked by heptanal even at the concentration of 0.001% dilution (1.9 nM; Figures 3H and 3I). The response strength increased at higher concentrations, saturating at ~1% dilution (1.9 μM in Figures 3H and 3I). By contrast, octanal evoked clear responses only at concentrations ≥0.1% (80 nM; Figure 3H, lower panel). Figure 3I shows the mean dose-response curves of I7 M/T cells to heptanal (n = 8 cells) and octanal (n = 7 cells). Based on the dose-response curves, the EC_{50} for heptanal (−7.91 ± 0.35 log molar; 12.3 nM) is significantly lower than that for octanal (−6.52 ± 0.12 log molar; 302.0 nM) (Figure 3J). These two values are also much lower than the respective values of I7 OSNs, supporting the role of olfactory mucus in enhancing the sensitivity of glomerular responses in vivo (Oka et al., 2006). In addition, the large convergence ratio for the projection from OSNs to M/T cells may increase the detection sensitivity of M/T cells.

Most importantly, these results show that I7 M/T cells can sensitively detect the cognate ligand of I7 within a broad range of concentrations. Resembling I7 OSNs, I7 M/T cells respond more sensitively to heptanal than to octanal in vivo. In fact, the difference in sensitivity to heptanal and octanal was further increased in M/T cells: the sensitivity to heptanal was ~25 times the sensitivity to octanal in M/T cells, whereas the difference was ~10 times in their presynaptic OSNs.

The Olfactory Tuning of I7 M/T Cells

The enhanced difference in sensitivity in I7 M/T cells suggests that the odor representation in M/T cells was sharpened rather than broadened by the intrabulbar circuitry following OSN input. To test this more directly, we used robotic olfactometer to present a large panel of odorants (69 odorants) of diverse molecular structures to probe the olfactory tuning curve of I7 M/T cells (Figure 3B; Table S1). In vivo studies on the olfactory tuning of M/T cells typically present all odorants at one fixed dilution of saturated vapor. Following this commonly adopted

approach, we diluted odorants to generate odorant pulses of saturated vapor of either 0.1% or 1% dilution. At 0.1% (~−6.7 log molar concentration for heptanal), M/T cells responded much more strongly to heptanal than to octanal, whereas at 1%, cells responded with similar strengths to heptanal and octanal (Figure 3I).

At 0.1% odorant dilution, the tuning curves of all I7 M/T cells recorded from different mice were highly selective and similar across cells (see Figure 4A for three examples; n = 9 cells). Heptanal elicited the strongest responses among 69 odorants in all cells. Sporadic responses to other odorants were observed but were not consistent across cells. When the odorant concentration was increased to 1%, the response tuning of M/T cells became broadened (Figure 4B; n = 10 cells). However, the overall shapes of the curves at these two concentrations were conserved (Figure 4C).

We quantified tuning curve sharpness by measuring lifetime sparseness (S), which has been used to describe the neuronal response selectivity in several sensory systems (Vinje and Gallant, 2000; Wilson et al., 2004). The mean S value of M/T cells was 0.84 ± 0.04 for odorants at 0.1% dilution, but it was reduced significantly to 0.66 ± 0.06 when the odorant concentrations were increased to 1% (Figure 4D). Nevertheless, even at the higher concentration, the tuning curve of M/T cells remained reasonably narrow (Figure 4C). M/T cells responded only to a few odorants out of 25 aldehydes tested at 1% dilution (Figure S2A). Although heptanal evoked vigorous responses from all I7 M/T cells, hexanal, which is just one carbon shorter than heptanal, elicited no responses from any I7 M/T cells.

To validate our results from dendritic recordings, we examined whether M/T cells randomly sampled with traditional recording methods exhibited similarly sharp tuning. We recorded M/T cells further away from the I7 glomerular area by lowering recording electrodes into the dorsal external plexiform layer and the mitral cell layer. These non-I7 M/T cells were activated and inhibited by only a fraction of odorants at 1% dilution (Figures S2B–S2G). In addition, mitral and tufted cells showed very similar tuning curves, and the S values for these two cell types were equally high (S = 0.85 ± 0.03 for mitral cells and 0.87 ± 0.03 for tufted cells) (Figures S2H and S2I), indicating that sharp tuning is a common property of M/T cells.

Because glomeruli have traditionally been considered computational units in the MOB (Mori et al., 1999; Shepherd et al., 2004), it is tempting to speculate that the tuning curves of M/T cells connecting to the same glomerulus are homogenous. Quantification revealed that the tuning curves were highly correlated among I7 M/T cells from different mice when odorant concentrations were low (Figure 4E, left panel). However, this correlation was weaker when odorant concentrations were increased (Figure 4E, right panel), suggesting that tuning curves of individual M/T cells become heterogeneous at high odorant concentrations.

To examine whether heptanal-evoked responses in I7 M/T cells can be broadened to nearby non-I7 M/T cells, we performed dendritic recordings from M/T cells that extended their primary dendrites to glomeruli adjacent to the I7 glomerulus (Figures 5A and 5B; n = 21 cells). These near-I7 M/T cells exhibited selective excitatory and inhibitory responses (Figures 5C and 5D). The majority of these cells were not excited by heptanal at any concentration tested (up to 10% dilution; n = 17 / 21 cells tested). Four of these non-I7 M/T cells responded to heptanal mildly even at concentrations ≥5% (9.5 μM), indicating the heptanal sensitivity of these neurons was ~600 times lower than that of I7 M/T cells (Figures 5E and 5F; EC_{50} = −5.14 ± 0.07 log molar or ~7.24 μM). This strongly suggests that the excitatory input from OSNs to a specific glomerulus does not disperse to M/T cells associated with neighboring glomeruli.

The Response Selectivity of Interneurons

Interneurons in the bulb outnumber M/T cells by a ratio of 100:1 (Shepherd et al., 2004). They are believed to exert strong effects on shaping the olfactory responses of M/T cells, but their olfactory tuning curves had not been systematically analyzed. A majority of interneurons in the glomerular layer are GABAergic PG cells, although some PG cells are dopaminergic (Maher and Westbrook, 2008). These cells receive excitatory inputs from OSNs, M/T cells, and short axon cells and are believed to inhibit lateral M/T cells (Aungst et al., 2003). We recorded from 28 PG cells with their dendritic arbors solely in the I7 glomerulus, without further differentiation of their neurotransmitter phenotypes (Figures 6A and 6B). Heptanal was typically the most effective stimulus among 69 odorants tested at both 0.1% and 1% dilution (Figures 6C–6E and S3A), but exceptions were observed for two PG cells at 1% dilution (see Figure 6D, upper panel). Unlike those of M/T cells, the tuning curves of I7 PG cells were broad at both 0.1% and 1% odorant dilutions (Figure 6E), resulting in low values of lifetime sparseness (Figure 6F). Non-I7 PG cells randomly sampled from the dorsal MOB also exhibited broad tuning curves (Figures S3B–S3E) and values of lifetime sparseness similar to those of I7 PG cells ($S = 0.59 \pm 0.11$ for non-I7 PG cells), suggesting that broad tuning is a general feature of PG cells. Unlike those of I7 M/T cells, the tuning curves of individual I7 PG cells were highly variable at both 0.1% and 1% dilutions (Figure 6E) and thus exhibited poor correlation between pairs of PG cells (Figure 6G).

Anatomical and physiological recordings in vitro have strongly suggested that granule cells provide the major mechanism of lateral inhibition among M/T cells (Arevian et al., 2008; Chen et al., 2000; Isaacson and Strowbridge, 1998; Jahr and Nicoll, 1982; Rall et al., 1966; Schoppa et al., 1998; Shepherd et al., 2004). The dendrites of granule cells form dendrodendritic synapses with the basal dendrites of M/T cells in the external plexiform layer. They may either receive inputs from a local subset of M/T cells and thus exhibit sharp tuning curves or integrate inputs from M/T cells within an extensive area and thus exhibit broad tuning curves. We randomly recorded and labeled granule cells by lowering electrodes into the granule cell layer of the dorsal MOB (Figures 7A and 7B). At 1% dilution, odorants evoked predominately excitatory responses from granule cells, although inhibitory responses were also occasionally observed (Figures 7C and 7D). Granule cells exhibit broad tuning curves (Figures 7E) and significantly lower lifetime sparseness values ($S = 0.56 \pm 0.11$) than randomly recorded M/T cells at the same concentration (Figure S4; $p < 0.05$, t test). By contrast, granule cells typically lacked any clear responses to odorants at 0.1% dilution (Figures 7E). The broad tuning suggests that granule cells integrate inputs from M/T cells corresponding to different OR types. Odorants at high concentrations may recruit additional glomeruli and thus become effective in activating granule cells. In addition, the concentration dependency of granule cell responses indicates that the function of lateral inhibition may become prominent at high odorant concentrations.

The Role of GABAergic Connections in Shaping Response Selectivity

$GABA_A$ receptors are widely expressed in M/T cells (Laurie et al., 1992; Nusser et al., 1999) and contribute to lateral inhibition mediated by reciprocal synapses between M/T cells and granule cells (Isaacson and Strowbridge, 1998; Jahr and Nicoll, 1982). Bicuculline, a $GABA_A$ receptor antagonist, blocks odor-evoked inhibitory responses in M/T cells (Margrie et al., 2001; Yokoi et al., 1995). However, the response profiles of OSNs presynaptic to the recorded M/T cells were unknown in these studies. Thus it remained unclear how inhibitory intrabulbar connections affect the responses of M/T cells to the ligands of their corresponding OR.

In order to explore the role of lateral inhibition in shaping odor representation, we examined the effects of blocking $GABA_A$ receptor on the response of I7 M/T cells to a series of aldehydes at different concentrations (Figure S5A–S5C). Prior to the application of bicuculline

methiodide (BMI), I7 M/T cells were excited by heptanal and octanal, but not five other odorants, at 0.1% dilution. Superfusion of BMI significantly enhanced the response strengths to heptanal and octanal at this concentration, but it did not produce any clear effect on the response to other odorants (Figures 8A and 8B). At 1% odorant dilution, I7 M/T cells responded to four out of the seven test odorants before BMI application. After BMI application, these cells were activated by all seven test odorants, and the increase in response strength was significant for six of the odorants (Figures 8C and 8D). BMI significantly reduced the value of lifetime sparseness only when odorants were tested at 1% but not at 0.1% (Figure 8E), suggesting that inhibitory networks in the MOB primarily sharpen odor representation in M/T cells at high concentrations.

Odorants at very high concentrations can produce very different perception quality from those at more behaviorally relevant concentrations (Gross-Isseroff and Lancet, 1988). At the concentration of 10% dilution, heptanal elicited different firing patterns from those detected at the concentrations of 0.1% and 1%. In contrast to vigorous firing throughout odorant pulses, I7 M/T cells exhibited an initial burst of high-frequency firing and then a period of silence (Figure 8F). BMI application unmasked strong firing of action potentials during the previously silent period (Figure 8F). Thus, GABAergic connections in the MOB may not only sharpen olfactory tuning mediated by lateral inhibition but also shut down M/T cells by self-inhibition when animals are challenged with odorants at high concentrations that are irrelevant to normal animal behaviors.

DISCUSSION

In order to study how the MOB transforms olfactory signals, we examined the response profiles of M/T cells and their presynaptic OSNs expressing a specific OR gene. We first characterized the response sensitivity and selectivity of OSNs expressing mouse I7 receptor (Figures 1 and 2). We then examined the response selectivity and olfactory tuning curves of M/T cells postsynaptic to I7 OSNs (Figures 3–5). To investigate the role of intrabulbar circuitry, we analyzed the olfactory tuning curves of interneurons and examined the effects of blocking inhibitory connections on the odor representation in M/T cells (Figures 6–8). Our data strongly indicate that M/T cells are narrowly tuned to the ligand of their corresponding OR, suggesting that olfactory information detected by an OR is channeled to an exclusive subset of M/T cells. In addition, our data reveal that lateral inhibition sharpens M/T cell tuning curves especially at high odorant concentrations. Below, we briefly discuss our evidence for these conclusions and their functional implications.

Odor Representation by M/T Cells in the MOB

It is generally believed that glomeruli function as computational units in the MOB. In each glomerulus, OSNs expressing a common OR form excitatory synapses with a small number of M/T cells, which then project to the downstream olfactory centers. With their extensive basal dendrites, M/T cells can interact laterally by forming reciprocal synapses with GABAergic interneurons in the glomerular layer and the external plexiform layer. This simple connection scheme has led to the popular assumption that the olfactory tuning of OSNs is propagated to M/T cells and further sharpened before being relayed to the olfactory cortex (Mori et al., 1999).

However, the exact relationship between the response profiles of OSNs and their postsynaptic M/T cells had not been directly tested in mammals. By applying a small number of odorants at arbitrarily determined concentrations, previous physiological studies have revealed that M/T cells can be excited by some odorants and inhibited by others (Margrie et al., 2001; Meredith, 1986; Wellis et al., 1989; Yokoi et al., 1995). By applying larger sets of odorants with diverse molecular features, two recent studies have shown that M/T cells respond selectively to

odorants at low concentrations (Davison and Katz, 2007; Fantana et al., 2008). However, it remains unknown whether the odorants that activate a M/T cell are indeed the ligands of its corresponding OR. In several other species, this may not be the case. For example, mitral cells in the zebrafish olfactory bulb respond broadly to odorants with intricate temporal patterns (Friedrich and Laurent, 2001). Similarly, odor representation is drastically broadened in the projection neurons of the *Drosophila* AL (Schlief and Wilson, 2007; Bhandawat et al., 2007; Wilson et al., 2004), an insect analog of the mammalian olfactory bulb. Without a direct comparison between the olfactory tuning of M/T cells and their corresponding presynaptic OSNs, it remains unclear whether a similar broadening scheme occurs in mammals.

Our approach was to compare the response profiles of the OSNs expressing I7 receptor and those of their postsynaptic M/T cells in mice. Our recordings demonstrate that I7 OSNs respond selectively to heptanal at low concentrations, but they are activated by several other aldehydes at a higher concentration. Consistently, I7 M/T cells respond selectively to heptanal at low concentrations but are excited by several other aldehydes that activate I7 OSNs at higher concentrations. The olfactory signals carried by I7 OSNs do not appear to disperse to M/T cells that are not directly associated with I7 glomeruli. For example, M/T cells that receive inputs from glomeruli adjacent to I7 glomeruli are not activated by heptanal at behaviorally relevant concentrations. These data indicate that M/T cells are primarily activated by odorants that are detected by their corresponding OSNs.

Differences in circuitry may explain why the strategy of odor representation in mice is distinct from those in the zebrafish and *Drosophila*. Zebrafish mitral cells extend multiple dendrites to receive inputs from several glomeruli, whereas mouse M/T cells receive their primary excitatory inputs from a single glomerulus (Mori et al., 1999; Yoshihara et al., 2001). Resembling M/T cells in the mice, a majority of projection neurons in the *Drosophila* AL have only one primary dendrite to receive inputs from a single glomerulus (Vosshall and Stocker, 2007; Wilson and Mainen, 2006). Imaging studies indicate that the responses of these projection neurons largely reflect the selectivity of their corresponding OSNs (Ng et al., 2002; Root et al., 2007; Wang et al., 2003). However, electrophysiological recordings demonstrate substantially broadened odor representation in the *Drosophila* AL (Wilson et al., 2004). The *Drosophila* olfactory system expresses a much smaller repertoire of ORs and contains fewer glomeruli. In addition, both excitatory and inhibitory lateral connections function in parallel in the *Drosophila* AL (Olsen et al., 2007; Olsen and Wilson, 2008; Shang et al., 2007), whereas lateral connections in the mammalian MOB are predominantly inhibitory (Egger and Urban, 2006; Shepherd et al., 2004; Wachowiak and Shipley, 2006). These differences in microcircuits may result in distinct coding strategies in the mammalian MOB and the insect AL.

In this study, we systematically studied only one genetically identified glomerulus. Because the I7→M71-GFP mouse line is currently the only one in which OSNs expressing an OR of known sensitive ligands project their axons to GFP-labeled glomeruli on the dorsal MOB, we have focused on analyzing the responses of I7 OSNs and their associated M/T cells and PG cells. Although our data from near-I7 M/T cells and randomly sampled bulbar neurons provide consistent views, firm generalization of our conclusion to other OR pathways requires further systematic characterization of OSNs and M/T cells associated with other genetically identified glomeruli.

One potential technical concern is whether dendritic recordings of I7 M/T cells accurately report the activity at the soma. Unlike many other types of neurons, M/T cells express active ion channels in their primary dendrites, and an action potential can be initiated either at the primary dendrite or at the soma (Chen et al., 1997). Typically, a weak or moderate stimulation of the olfactory nerve layer results in spike initiation at the soma, whereas a high-intensity

electrical stimulation of ONL results in spike initiation at the dendritic trunk (Chen et al., 1997, 2002; Shen et al., 1999). Action potentials initiated at the soma of a M/T cell can be reliably back-propagated to its primary dendrite even at high firing frequencies (Chen et al., 1997, 2002; Shen et al., 1999). Similarly, action potentials initiated at the dendritic trunk of a M/T cell reliably reach the soma under normal physiological conditions (Chen et al., 1997, 2002; Shen et al., 1999). If our recorded signals only reflected the activity of OSNs but not the effect of lateral connections, we should not be able to observe inhibitory responses. However, we had observed both excitatory and inhibitory spiking responses at the dendritic trunk (Figures 4 and 5) and significant effects of bicuculline on the responses of I7 M/T cells (Figure 8). These observations indicate that the spiking signals we recorded were most likely initiated at the somata and back-propagated to the primary dendrites. Thus, previous studies and our recordings in this study argue strongly that dendritic spikes accurately match with the firing activity at the soma.

Another potential technical concern arises from our choice of urethane as the anesthetic, which has been used in many in vivo physiological studies of the MOB. Compared with other anesthetics such as ketamine or isoflurane, the effects of urethane on olfactory responses appear small. Ketamine is an NMDA receptor antagonist that can dramatically reduce dendrodendritic lateral inhibition in the MOB (Chen et al., 2000; Isaacson and Strowbridge, 1998; Schoppa et al., 1998), leading to decreased selectivity in responses of M/T cells (Rinberg et al., 2006). Isoflurane and other volatile anesthetics activate many odorant receptors and thus can have undesirable effects on the responses to test odorants (Peterlin et al., 2005). It has been reported that urethane induces up- and down-states in global brain activity and thus affects the strength of dendrodendritic synapses in the MOB (Tsuno et al., 2008). However, urethane-induced changes in global activity appear to modulate the olfactory responses in the olfactory cortex but not in the bulb (Murakami et al., 2005). In this study, we have not recorded cortical EEG to differentiate these two stages. Future recordings from the MOB of behaving mice may shed light on the more subtle effects of global brain activity on M/T cell responses.

Role of the Intrabulbar Circuit in Shaping MOB Output

A vast majority of neurons in the MOB are GABAergic and inhibitory interneurons. PG cells in the glomerular layer are believed to provide center-surround inhibition among glomeruli (Aungst et al., 2003). GABAergic granule cells receive excitatory inputs from the axonal collaterals of nearby M/T cells (Schoppa, 2009; Schoppa et al., 1998) and form reciprocal dendrodendritic synapses with M/T cells in the external plexiform layer (Chen et al., 2000; Isaacson and Strowbridge, 1998; Schoppa et al., 1998; Shepherd et al., 2004), thus providing another layer of lateral inhibition. Consistently, an early experiment showed that rabbit M/T cells are typically inhibited by odorant molecules with structures closely related to their excitatory odorant molecules and application of bicuculline suppresses the odor-evoked inhibition (Yokoi et al., 1995). In another case, odorant-evoked inhibition even switched to excitation following the application of bicuculline (Margrie et al., 2001).

However, the extent to which lateral inhibition shapes the odor representation in M/T cells remains controversial (Valley and Firestein, 2008). By combining intracellular recordings and imaging, Luo and Katz observed inhibition of M/T cells by many odorants that activate surrounding glomeruli (Luo and Katz, 2001). Using extracellular recording and imaging with a large number of odorants, Fantana et al. recently showed that M/T cells respond to only a small number of odorants in terms of either excitation or inhibition (Fantana et al., 2008). By combining recordings and photostimulation of M/T cells, Arenkiel et al. concluded that a mitral cell is excited exclusively by a single glomerulus but not inhibited by other glomeruli (Arenkiel et al., 2007). Notably, these observations may have been produced by different recording techniques, numbers of odorant stimuli, and odorant intensities. Because odor space consists

of high dimensions whereas glomeruli are organized into two dimensions, it is unclear whether lateral inhibition plays any role in sharpening odor representation in M/T cells (Laurent, 1999).

By superfusion of bicuculline in vivo, we find that blocking GABAergic transmissions exerts differential effects on the responses of I7 M/T cells to odorants at two concentrations (Figure 8). Bicuculline increases response strength but does not affect response selectivity when the odorant concentration is low. When odorant concentration is increased, bicuculline reduces response selectivity, suggesting that lateral inhibition may sharpen odor representation by suppressing the weakly excitatory responses of M/T cells to nonoptimal odorants at high concentrations. Consistently, granule cells are activated by odorants at high but not low concentrations, suggesting a critical role of granule cells in providing concentration-dependent lateral inhibition. Nevertheless, PG cells and granule cells do not respond uniformly to all odorants. In addition, inhibitory responses, defined as odorant-evoked reduction of basal firing in M/T cells, were observed following exposure to 10%–40% of odorants even at the concentration of 1% dilution (Figure S2). The selectivity of inhibitory responses is consistent with the proposal that a M/T cell may receive strong inhibitory responses only from a sparse subset of glomeruli (Fantana et al., 2008;Soucy et al., 2009;Willhite et al., 2006).

The tuning curves of individual M/T cells associated with the same glomerulus become heterogeneous at higher odorant concentrations (Figure 4). In addition, PG cells associated with the same glomerulus respond broadly and heterogeneously, possibly because they receive input from different short axon cells in addition to their common glomerular inputs (Wachowiak and Shipley, 2006) (Figure S5D). We speculate that individual M/T cells associated with the same glomerulus may interact with different sets of interneurons, including PG cells and granule cells (Figure S5D). Therefore, although glomeruli have been traditionally considered computation units of the MOB, intrabulbar circuitry may produce heterogeneous responses from individual M/T cells associated with the same glomerulus and thus relay olfactory information to downstream centers through a larger number of channels.

Our data do not exclude the possibility that inhibitory connections may have functions other than sharpening odor representation in M/T cells. Oscillatory firing among M/T cells can have strong effects on downstream processing in the olfactory cortex (Poo and Isaacson, 2009). Inhibitory lateral connections in the MOB may regulate the synchronized firing of M/T cells, thus further contributing to the sparse representation of olfactory signals in the olfactory cortex (Stettler and Axel, 2009). Finally, the mammalian MOB receives strong centrifugal modulatory inputs from the brainstem, basal forebrain, and olfactory cortex (Shepherd et al., 2004; Shipley and Ennis, 1996; Willhite et al., 2006). These centrifugal inputs may modulate the strength of lateral inhibition, thus producing dynamic odor representation in the context of different behavioral states in a given animal (Kay and Laurent, 1999).

EXPERIMENTAL PROCEDURES

Animals

Animal care and use were carried out following institutional policy of the National Institute of Biological Sciences, Beijing, and of the University of Pennsylvania. Adult mI7→M71-IRES-tauGFP mice (6–12 weeks, 18–30 g) of either sex were used for in vivo recordings, and mice at younger age (4–6 weeks) were used for recordings from the OSNs. In these mice, the M71 receptor was replaced with the mouse I7 (mI7) receptor. In addition, tauGFP was coexpressed with the mI7 receptor using bicistronic strategy (Bozza et al., 2002). For simplicity we denoted these mice as mI7→M71-GFP mice, I7-expressing OSNs in these mice as I7 OSNs, GFP^+ glomeruli as I7 glomeruli, and the M/T cells directly associated with the GFP^+ glomeruli as I7 M/T cells.

Recordings from the MOE

Electrophysiology—Recordings from OSNs were carried out in an intact epithelial preparation following previously published procedures (Grosmaitre et al., 2006). Briefly, mI7→M71-GFP mice were deeply anesthetized with ketamine and then decapitated. Following a brief immersion of the head in icy Ringer's solution (containing in mM: 124 NaCl, 3 KCl, 1.3 $MgSO_4$, 2 $CaCl_2$, 26 $NaHCO_3$, 1.25 NaH_2PO_4, 5.5 glucose, and 4.47 sucrose; 305 mOsm and pH = 7.4 bubbled with 95% O_2 and 5% CO_2), the nose was dissected out en bloc and the olfactory mucosa was peeled off and kept in oxygenated Ringer's solution. Before recording, the tissue was transferred to a recording chamber with the mucus layer facing up and then continuously perfused with oxygenated Ringer's solution at 25°C±2°C. The dendritic knobs of I7 OSNs were identified by green fluorescence in both knob and cilia and then further visualized through an upright differential interference contrast (DIC) microscope (Olympus BX51WI), which was equipped with a 40× water-immersion objective and an accessory lens for an additional 4× magnification. Cell-attached recordings were performed on the dendritic knobs with a glass recording pipette, which was filled with the following solution (in mM): 70 KCl, 53 KOH, 30 methanesulfonic acid, 5 EGTA, 10 HEPES, and 70 sucrose, pH 7.2 (310 mOsm). We started recordings only after the glass-pipette formed a Giga-seal with the dendritic knob membrane. Recordings were controlled by an EPC-10 amplifier combined with the Pulse software (Heka Electronik). Odorant stimuli were delivered by Picospritzer (Pressure System IIe, Toohey Company)-controlled pressure ejection from a seven-barrel pipette that was placed ~50 μm downstream from the recording site. All odorants (Sigma) were diluted with Ringer's solution from a 0.5 M stock solution in dimethyl sulfoxide (DMSO).

Data Analysis—The details of quantifying the odorant responses of OSNs are described elsewhere (Rospars et al., 2003). Odorant responses of OSNs usually consisted of a burst of multiple action potentials. For odorants at high concentrations, this burst was typically followed by a period of silence and then a secondary increase in spiking activity. Because odorant properties are better encoded by the initial response (Rospars et al., 2003), we focused on analyzing this initial response of the poststimulus activity against a background of spontaneous firing properties. The basal firing frequency of OSNs (F_θ) was calculated by analyzing the median instantaneous firing frequency of the spontaneous activity recorded for at least 60 s before odorant delivery. The response of a cell to an odorant was defined as firing of action potentials with instantaneous firing frequency higher than the threshold value (F_θ + 1.5 spikes/s) within the time window of 2 s after stimulus onset. The bursting response typically occurs immediately after the application of an effective odorant, resulting in a time window less than 500 ms for most responses. The amplitude of the odorant responses (F_i) was quantified as the median value of the instantaneous frequencies of the initial burst that exhibited a sufficient increase in firing frequency as compared to the threshold value. An OSN was considered nonresponsive to an odorant (F_i = 0) if the number of action potentials within the initial burst was less than four or the overall mean firing rate following odorant application was less than the mean basal rate.

Recordings from the MOB

For anesthesia, mice were injected with atropine (0.05 mg/kg) and then urethane i.p. (1.64 g/kg, 20%). Animals were then mounted in a stereotaxic apparatus and kept warm (39° C) with an electric heating pad (BrainKing Biotech, Beijing, China). The respiratory cycles of the animals were monitored with a strain gauge affixed to chest skin. Signals were amplified by a custom-made strain gauge amplifier and further band-pass (0.1~20 Hz) filtered by a Brownlee 440 amplifier.

In Vivo Electrophysiology and Two-Photon Imaging—The skull above the dorsal surface of the olfactory bulb was thinned, and the GFP^+ glomerulus was identified under a

fluorescent stereo zoom microscope (Olympus SZX12) (Figure S1A). A small hole was opened above the green glomerulus with the dura mater remaining intact. Mice were then transferred onto a custom-made 2D stage under a two-photon microscope (Olympus FV1000). I7 glomeruli were visualized with two-photon microscopy using a 40× water-immersion objective (N.A. = 0.8). Fluorescence was generated using two-photon excitation by a mode-locked Ti-sapphire laser (Chameleon Ultra, Coherent) operating at 140 fs pulse width and 910–1040 nm wavelength. Images were acquired using the Olympus Fluoview software.

For recordings of I7 M/T cells and PG cells, borosilicate microelectrodes (resistance 10~20 MΩ) were pulled on a Sutter horizontal puller (P-97, Sutter Instrument) and filled with 1 M sodium chloride and 4% neurobiotin (Vector Laboratories). A fluorescent marker (1% Lucifer yellow from Sigma-Aldrich or 3KD tetramethylrhodamine dextran amines from Invitrogen) was added into the intrapipette solution to visualize the pipette tip. Under the guidance of two-photon imaging, a recording pipette was targeted toward an I7 glomerulus with an angle of 30° to the pial surface (Figure 3C). We started the search for extracellular single units when the tip of the recording pipette reached the I7 glomerulus. After we isolated a single-unit with signal/noise ratio >10, electrophysiological signals were amplified (Axoclamp 2B, Axon Instruments), band-pass filtered at 0.5–3 KHz (Brownlee Amplifier model 440), and then digitized at 8 kHz. Respiratory rhythms and field potentials were simultaneously acquired for offline analysis. The recording depths suggest that a majority of I7 M/T cells were recorded extracellularly from their primary dendritic trunks. However, some I7 external tufted cells and PG cells might have been recorded from their somata that surrounded the I7 glomerulus. Randomly sampled M/T cells and granule cells were recorded extracellularly by lowering the recording electrodes into specific layers where their corresponding somata were located. Data acquisition and experimental control were implemented by custom-written software using driver programs provided by National Instruments. (−)-Bicuculline methiodide (Sigma) was applied by superfusion through a custom-built chamber that was sealed to the cranium.

Odorant Delivery—Room air was filtered with active charcoal and then presented continuously in front of mouse nostrils at a constant flow rate of 4 l/min. Odorants were delivered with a robotic arm or a custom-made seven-channel olfactometer (Figure 3B). Odorants were stored in headspace vials with different dilutions in mineral oil. For robotic delivery, a 3D robotic arm (I&J7200C) was used to access odorants from an 8 × 8 odorant panel, which included odorants of diverse functional groups and carbon-chain lengths. A seven-channel olfactometer was used to deliver highly volatile aldehydes in order to reduce cross-contamination between odorants. In total, 69 odorants plus two controls were used to map the olfactory tuning curve. A complete list of test odorants and their molar concentrations at 1% dilutions can be found in Table S1. Odorized air was delivered with adjustable flow rates into the continuous air stream for further dilution. Flow rates were controlled by flowmeters (Botion LZB-2) and monitored digitally (FMA 1700/1800 series, Omega). To ensure accuracy in the timing of odorant delivery, odorants were diverted into the vacuum for the first 1 s and then delivered to the mouse nostril by switching open a three-way solenoid valve (Parker) for 2 s. An additional stream of clean air (200 ml/min) was injected into the solenoid valve 3 s after the termination of odorant pulses to minimize residual odorant from previous trials. Intertrial intervals were at least 15 s to reduce habituation. Teflon tubing was used to reduce cross-contamination.

The molar concentration of an odorant was calculated based on the ideal gas law $n = pV/RT$, in which p is the saturated vapor pressure at room temperature, V is the volume, R is the gas constant, and T is the absolute temperature.

Histology—After recordings, neurons were labeled using a juxtacellular labeling technique that has been described in detail elsewhere (Pinault, 1996). Briefly, neurobiotin in a recording

pipette (4%) was electrophoresized into neurons with small positive currents (<10 nA; 0.2 s on/0.2 s off) for a maximum of 10 min. The amplitudes of the injected currents were adjusted so that the evoked firing of action potentials was tightly synchronized with current injection. After recovery of at least 1 hr, mice were sacrificed with an overdose of pentobarbiturate, perfused by 4% paraformaldehyde in phosphate-buffered saline with 0.2% picric acid and then postfixed for at least 4 hr at room temperature. After cryoprotection in 30% sucrose, coronal sections (40–60 μm) were prepared with a freezing cryostat (Leica CR 1900). Sections were visualized with Cy3-streptavidin (1:500, Jackson Immunoresearch) and then mounted with 50% glycerol containing DAPI to counterstain cell nuclei. Fluorescent images were collected by a laser-scanning confocal microscope (Zeiss LSM 510 Meta) with a 20× or 40× air objective. Images were reconstructed using Adobe Photoshop. Glomeruli and layers were delineated by DAPI staining.

Occasionally (<10% of cases), two or a few cells were dye labeled after juxtacellular labeling. For M/T cells and PG cells, only data from single-cell labeling were accepted for further analysis. In a few cases, multiple labeling of granule cells were used (for example, Figure 7B) because our sole purpose for granule cells was to identify the cell type.

Data Analysis—Data analysis was carried out using custom-written programs in Matlab (Math-works). Recordings were confirmed to be from single units by clean refractory periods within the autocorrelograms of recorded spiking trains (Figures S1C and S1D). PSTHs were computed by counting the number of action potentials within sequential time bins (300–500 ms duration). To calculate the breathing-triggered PSTH during odorant application (Figure S1E), electrophysiological traces were divided in segments based on respiratory cycles, and all segments were normalized to the same length. The PSTH was calculated individually for each segment and then averaged across segments.

The response strength of a cell to an odorant was first calculated by subtracting the spontaneous rate (2 s preceding odorant initiation) from the firing rate during the odorant application within each trial and then averaging across trials. Because control stimuli (pure air or air from the mineral oil) occasionally elicited weak responses from some cells (Grosmaitre et al., 2007), we further subtracted the value of response strength to controls from that of the cell to odorants. Thus, positive values of response strength indicate excitation and negative ones represent inhibition. After analyzing the olfactory response of M/T cells by incorporating their temporal features, a recent study showed that the mean firing rate in each respiratory cycle can robustly encode information of odor identity and concentration (Bathellier et al., 2008). Because the odor pulse duration was fixed and each animal exhibited a rather stable respiratory rhythm during recordings in this study, the analyses by Bathellier et al. support the validity of measuring response strength using the difference in firing rates (Bathellier et al., 2008).

To plot the dose-response curves, normalized response strength was first calculated as “the response strength at a specific concentration/maximum response strength across all concentrations” and then averaged across cells from different groups. Dose-response curves were fit to a sigmoid function: $f(x) = 1/(1+exp(-a \times (x - b)))$, where x represents the mean normalized response strength of the cells at a specific concentration, a, slope, and b, EC_{50}. To plot the mean tuning curves, the response strengths of the cell to all odorants were first normalized to the maximal response of this cell and the tuning curves of all cells from a specific experimental group were averaged. We arranged the values of response strengths against all odorants along the x axis so that the strongest excitatory response was in the middle of the curve and weak or inhibitory responses were at both ends. The alignments of the odorant identities for I7 M/T cells and PG cells are listed in Table S2.

The response selectivity to a set of odorants was quantified by calculating the lifetime sparseness using nonparametric statistics (Vinje and Gallant, 2000). Lifetime sparseness $S = \left\{1 - (\Sigma r_i/N)^2/\Sigma\left(r_i^2/N\right)\right\} / [1 - (1/N)]$, where r_i is the response strength to odor i and N is the total number of the stimuli. Any negative values of r_i were set to zero before computing lifetime sparseness. S measures the peakedness of a response distribution. Values of S near 0 indicate a flat distribution of the responses to various odorants, and values near 1 indicate a sparse distribution of responses to the stimulus set. The similarity between the tuning curves of two cells was calculated using Pearson's correlation coefficient for their tuning curves. The correlation matrices shown in Figures 4E and 6G represent the color-coded coefficients between any two cells tested with the same concentrations.

Supplementary Material

Refer to Web version on PubMed Central for supplementary material.

Acknowledgments

We thank Peter Mombaerts (MPI, Frankfurt, Germany) and Thomas Bozza (NWU, Evanston, IL, USA) for mI7→/M71-IRES-tauGFP mice and C. Zhan at NIBS imaging facility for technical assistance. M.L. is supported by China Ministry of Science and Technology 863 and 973 Grants, a China NSFC Young Investigator Grant and a Human Frontier Science Program grant. M.M. is supported by NIDCD, NIH.

REFERENCES

Araneda RC, Kini AD, Firestein S. The molecular receptive range of an odorant receptor. Nat. Neurosci 2000;3:1248–1255. [PubMed: 11100145]

Arenkiel BR, Peca J, Davison IG, Feliciano C, Deisseroth K, Augustine GJ, Ehlers MD, Feng G. *In vivo* light-induced activation of neural circuitry in transgenic mice expressing channelrhodopsin-2. Neuron 2007;54:205–218. [PubMed: 17442243]

Arevian AC, Kapoor V, Urban NN. Activity-dependent gating of lateral inhibition in the mouse olfactory bulb. Nat. Neurosci 2008;11:80–87. [PubMed: 18084286]

Aungst JL, Heyward PM, Puche AC, Karnup SV, Hayar A, Szabo G, Shipley MT. Centre-surround inhibition among olfactory bulb glomeruli. Nature 2003;426:623–629. [PubMed: 14668854]

Bathellier B, Buhl DL, Accolla R, Carleton A. Dynamic ensemble odor coding in the mammalian olfactory bulb: sensory information at different timescales. Neuron 2008;57:586–598. [PubMed: 18304487]

Belluscio L, Lodovichi C, Feinstein P, Mombaerts P, Katz LC. Odorant receptors instruct functional circuitry in the mouse olfactory bulb. Nature 2002;419:296–300. [PubMed: 12239567]

Bhandawat V, Olsen SR, Gouwens NW, Schlief ML, Wilson RI. Sensory processing in the Drosophila antennal lobe increases reliability and separability of ensemble odor representations. Nat. Neurosci 2007;10:1474–1482. [PubMed: 17922008]

Bozza T, Feinstein P, Zheng C, Mombaerts P. Odorant receptor expression defines functional units in the mouse olfactory system. J. Neurosci 2002;22:3033–3043. [PubMed: 11943806]

Buck L, Axel R. A novel multigene family may encode odorant receptors: a molecular basis for odor recognition. Cell 1991;65:175–187. [PubMed: 1840504]

Chen WR, Midtgaard J, Shepherd GM. Forward and backward propagation of dendritic impulses and their synaptic control in mitral cells. Science 1997;278:463–467. [PubMed: 9334305]

Chen WR, Xiong W, Shepherd GM. Analysis of relations between NMDA receptors and GABA release at olfactory bulb reciprocal synapses. Neuron 2000;25:625–633. [PubMed: 10774730]

Chen WR, Shen GY, Shepherd GM, Hines ML, Midtgaard J. Multiple modes of action potential initiation and propagation in mitral cell primary dendrite. J. Neurophysiol 2002;88:2755–2764. [PubMed: 12424310]

Davison IG, Katz LC. Sparse and selective odor coding by mitral/tufted neurons in the main olfactory bulb. J. Neurosci 2007;27:2091–2101. [PubMed: 17314304]

Duchamp-Viret P, Chaput MA, Duchamp A. Odor response properties of rat olfactory receptor neurons. Science 1999;284:2171–2174. [PubMed: 10381881]

Egger V, Urban NN. Dynamic connectivity in the mitral cell-granule cell microcircuit. Semin. Cell Dev. Biol 2006;17:424–432. [PubMed: 16889994]

Fantana AL, Soucy ER, Meister M. Rat olfactory bulb mitral cells receive sparse glomerular inputs. Neuron 2008;59:802–814. [PubMed: 18786363]

Friedrich RW, Laurent G. Dynamic optimization of odor representations by slow temporal patterning of mitral cell activity. Science 2001;291:889–894. [PubMed: 11157170]

Grosmaitre X, Vassalli A, Mombaerts P, Shepherd GM, Ma M. Odorant responses of olfactory sensory neurons expressing the odorant receptor MOR23: a patch clamp analysis in gene-targeted mice. Proc. Natl. Acad. Sci. USA 2006;103:1970–1975. [PubMed: 16446455]

Grosmaitre X, Santarelli LC, Tan J, Luo M, Ma M. Dual functions of mammalian olfactory sensory neurons as odor detectors and mechanical sensors. Nat. Neurosci 2007;10:348–354. [PubMed: 17310245]

Gross-Isseroff R, Lancet D. Concentration-dependent changes of perceived odor quality. Chem. Senses 1988;13:191–204.

Isaacson JS, Strowbridge BW. Olfactory reciprocal synapses: dendritic signaling in the CNS. Neuron 1998;20:749–761. [PubMed: 9581766]

Jahr CE, Nicoll RA. An intracellular analysis of dendrodendritic inhibition in the turtle *in vitro* olfactory bulb. J. Physiol 1982;326:213–234. [PubMed: 7108788]

Kay LM, Laurent G. Odor- and context-dependent modulation of mitral cell activity in behaving rats. Nat. Neurosci 1999;2:1003–1009. [PubMed: 10526340]

Krautwurst D, Yau KW, Reed RR. Identification of ligands for olfactory receptors by functional expression of a receptor library. Cell 1998;95:917–926. [PubMed: 9875846]

Laurent G. A systems perspective on early olfactory coding. Science 1999;286:723–728. [PubMed: 10531051]

Laurie DJ, Seeburg PH, Wisden W. The distribution of 13 GABAA receptor subunit mRNAs in the rat brain. II. Olfactory bulb and cerebellum. J. Neurosci 1992;12:1063–1076. [PubMed: 1312132]

Luo M, Katz LC. Response correlation maps of neurons in the mammalian olfactory bulb. Neuron 2001;32:1165–1179. [PubMed: 11754845]

Maher BJ, Westbrook GL. Co-transmission of dopamine and GABA in periglomerular cells. J. Neurophysiol 2008;99:1559–1564. [PubMed: 18216231]

Malnic B, Hirono J, Sato T, Buck LB. Combinatorial receptor codes for odors. Cell 1999;96:713–723. [PubMed: 10089886]

Margrie TW, Sakmann B, Urban NN. Action potential propagation in mitral cell lateral dendrites is decremental and controls recurrent and lateral inhibition in the mammalian olfactory bulb. Proc. Natl. Acad. Sci. USA 2001;98:319–324. [PubMed: 11120888]

Meredith M. Patterned response to odor in mammalian olfactory bulb: the influence of intensity. J. Neurophysiol 1986;56:572–597. [PubMed: 3537224]

Mombaerts P, Wang F, Dulac C, Chao SK, Nemes A, Mendelsohn M, Edmondson J, Axel R. Visualizing an olfactory sensory map. Cell 1996;87:675–686. [PubMed: 8929536]

Mori K, Nagao H, Yoshihara Y. The olfactory bulb: coding and processing of odor molecule information. Science 1999;286:711–715. [PubMed: 10531048]

Murakami M, Kashiwadani H, Kirino Y, Mori K. State-dependent sensory gating in olfactory cortex. Neuron 2005;46:285–296. [PubMed: 15848806]

Ng M, Roorda RD, Lima SQ, Zemelman BV, Morcillo P, Miesenböck G. Transmission of olfactory information between three populations of neurons in the antennal lobe of the fly. Neuron 2002;36:463–474. [PubMed: 12408848]

Nusser Z, Sieghart W, Mody I. Differential regulation of synaptic GABAA receptors by cAMP-dependent protein kinase in mouse cerebellar and olfactory bulb neurones. J. Physiol 1999;521:421–435. [PubMed: 10581313]

Oka Y, Katada S, Omura M, Suwa M, Yoshihara Y, Touhara K. Odorant receptor map in the mouse olfactory bulb: *in vivo* sensitivity and specificity of receptor-defined glomeruli. Neuron 2006;52:857–869. [PubMed: 17145506]

Olsen SR, Wilson RI. Lateral presynaptic inhibition mediates gain control in an olfactory circuit. Nature 2008;452:956–960. [PubMed: 18344978]

Olsen SR, Bhandawat V, Wilson RI. Excitatory interactions between olfactory processing channels in the Drosophila antennal lobe. Neuron 2007;54:89–103. [PubMed: 17408580]

Peterlin Z, Ishizawa Y, Araneda R, Eckenhoff R, Firestein S. Selective activation of G-protein coupled receptors by volatile anesthetics. Mol. Cell. Neurosci 2005;30:506–512. [PubMed: 16185894]

Pinault D. A novel single-cell staining procedure performed in vivo under electrophysiological control: morpho-functional features of juxtacellularly labeled thalamic cells and other central neurons with biocytin or Neurobiotin. J. Neurosci. Methods 1996;65:113–136. [PubMed: 8740589]

Poo C, Isaacson JS. Odor representations in olfactory cortex: “sparse” coding, global inhibition, and oscillations. Neuron 2009;62:850–861. [PubMed: 19555653]

Rall W, Shepherd GM, Reese TS, Brightman MW. Dendrodendritic synaptic pathway for inhibition in the olfactory bulb. Exp. Neurol 1966;14:44–56. [PubMed: 5900523]

Ressler KJ, Sullivan SL, Buck LB. Information coding in the olfactory system: evidence for a stereotyped and highly organized epitope map in the olfactory bulb. Cell 1994;79:1245–1255. [PubMed: 7528109]

Rinberg D, Koulakov A, Gelperin A. Sparse odor coding in awake behaving mice. J. Neurosci 2006;26:8857–8865. [PubMed: 16928875]

Root CM, Semmelhack JL, Wong AM, Flores J, Wang JW. Propagation of olfactory information in Drosophila. Proc. Natl. Acad. Sci. USA 2007;104:11826–11831. [PubMed: 17596338]

Rospars JP, Lánský P, Duchamp A, Duchamp-Viret P. Relation between stimulus and response in frog olfactory receptor neurons *in vivo*. Eur. J. Neurosci 2003;18:1135–1154. [PubMed: 12956713]

Rubin BD, Katz LC. Optical imaging of odorant representations in the mammalian olfactory bulb. Neuron 1999;23:499–511. [PubMed: 10433262]

Schlief ML, Wilson RI. Olfactory processing and behavior downstream from highly selective receptor neurons. Nat. Neurosci 2007;10:623–630. [PubMed: 17417635]

Schoppa NE. Inhibition acts globally to shape olfactory cortical tuning. Neuron 2009;62:750–752. [PubMed: 19555643]

Schoppa NE, Kinzie JM, Sahara Y, Segerson TP, Westbrook GL. Dendrodendritic inhibition in the olfactory bulb is driven by NMDA receptors. J. Neurosci 1998;18:6790–6802. [PubMed: 9712650]

Shang Y, Claridge-Chang A, Sjulson L, Pypaert M, Miesenböck G. Excitatory local circuits and their implications for olfactory processing in the fly antennal lobe. Cell 2007;128:601–612. [PubMed: 17289577]

Shen GY, Chen WR, Midtgaard J, Shepherd GM, Hines ML. Computational analysis of action potential initiation in mitral cell soma and dendrites based on dual patch recordings. J. Neurophysiol 1999;82:3006–3020. [PubMed: 10601436]

Shepherd, GM.; Chen, WR.; Greer, CA. Olfactory Bulb. In: Shepherd, GM., editor. The Synaptic Organization of the Brain. Oxford University Press; New York: 2004. p. 165-217.

Shipley MT, Ennis M. Functional organization of olfactory system. J. Neurobiol 1996;30:123–176. [PubMed: 8727988]

Soucy ER, Albeanu DF, Fantana AL, Murthy VN, Meister M. Precision and diversity in an odor map on the olfactory bulb. Nat. Neurosci 2009;12:210–220. [PubMed: 19151709]

Stettler DD, Axel R. Representations of odor in the piriform cortex. Neuron 2009;63:854–864. [PubMed: 19778513]

Tsuno Y, Kashiwadani H, Mori K. Behavioral state regulation of dendrodendritic synaptic inhibition in the olfactory bulb. J. Neurosci 2008;28:9227–9238. [PubMed: 18784303]

Uchida N, Takahashi YK, Tanifuji M, Mori K. Odor maps in the mammalian olfactory bulb: domain organization and odorant structural features. Nat. Neurosci 2000;3:1035–1043. [PubMed: 11017177]

Valley MT, Firestein S. A lateral look at olfactory bulb lateral inhibition. Neuron 2008;59:682–684. [PubMed: 18786352]

Vassar R, Chao SK, Sitcheran R, Nuñez JM, Vosshall LB, Axel R. Topographic organization of sensory projections to the olfactory bulb. Cell 1994;79:981–991. [PubMed: 8001145]

Vinje WE, Gallant JL. Sparse coding and decorrelation in primary visual cortex during natural vision. Science 2000;287:1273–1276. [PubMed: 10678835]

Vosshall LB, Stocker RF. Molecular architecture of smell and taste in Drosophila. Annu. Rev. Neurosci 2007;30:505–533. [PubMed: 17506643]

Wachowiak M, Cohen LB. Representation of odorants by receptor neuron input to the mouse olfactory bulb. Neuron 2001;32:723–735. [PubMed: 11719211]

Wachowiak M, Shipley MT. Coding and synaptic processing of sensory information in the glomerular layer of the olfactory bulb. Semin. Cell Dev. Biol 2006;17:411–423. [PubMed: 16765614]

Wang JW, Wong AM, Flores J, Vosshall LB, Axel R. Two-photon calcium imaging reveals an odor-evoked map of activity in the fly brain. Cell 2003;112:271–282. [PubMed: 12553914]

Wellis DP, Scott JW, Harrison TA. Discrimination among odorants by single neurons of the rat olfactory bulb. J. Neurophysiol 1989;61:1161–1177. [PubMed: 2746317]

Willhite DC, Nguyen KT, Masurkar AV, Greer CA, Shepherd GM, Chen WR. Viral tracing identifies distributed columnar organization in the olfactory bulb. Proc. Natl. Acad. Sci. USA 2006;103:12592–12597. [PubMed: 16895993]

Wilson RI, Mainen ZF. Early events in olfactory processing. Annu. Rev. Neurosci 2006;29:163–201. [PubMed: 16776583]

Wilson RI, Turner GC, Laurent G. Transformation of olfactory representations in the Drosophila antennal lobe. Science 2004;303:366–370. [PubMed: 14684826]

Yokoi M, Mori K, Nakanishi S. Refinement of odor molecule tuning by dendrodendritic synaptic inhibition in the olfactory bulb. Proc. Natl. Acad. Sci. USA 1995;92:3371–3375. [PubMed: 7724568]

Yoshihara Y, Nagao H, Mori K. Neurobiology. Sniffing out odors with multiple dendrites. Science 2001;291:835–837. [PubMed: 11225631]

Zhang X, Zhang X, Firestein S. Comparative genomics of odorant and pheromone receptor genes in rodents. Genomics 2007;89:441–450. [PubMed: 17303377]

Zhao H, Ivic L, Otaki JM, Hashimoto M, Mikoshiba K, Firestein S. Functional expression of a mammalian odorant receptor. Science 1998;279:237–242. [PubMed: 9422698]

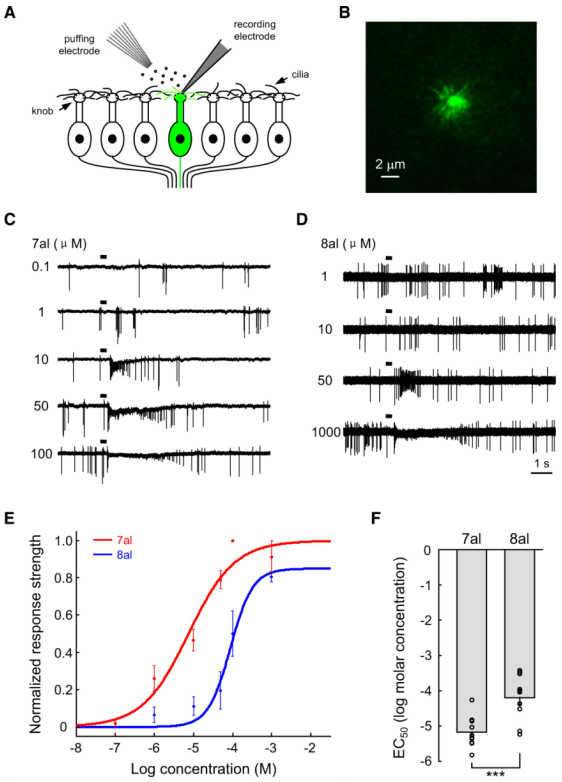

Figure 1. I7 OSNs Respond ~10 Times More Sensitively to Heptanal than to Octanal

(A) Schematic representation of experimental strategy. I7 OSNs (green) were identified by green fluorescence in an intact epithelial preparation. Their firing of action potentials was recorded extracellularly from dendritic knobs in cell-attached mode. Odorants were applied by pressure through a seven-barrel pipette.

(B) Strong green fluorescence in the dendritic knob and cilia of a GFP^+ I7 OSN.

(C) Traces showing the responses evoked by heptanal at different concentrations as indicated by the numbers to the left (in µM). Horizontal bars indicate the timing of odorant application (300 ms). In this and the following figures, heptanal is abbreviated as 7al and octanal as 8al.

(D) Reponses of another I7 OSN to octanal at different concentrations.

(E) Dose-response plots and fitted sigmoid functions of I7 OSNs to heptanal (n = 10 cells) and octanal (n = 10 cells). The response strength was normalized to the mean saturated firing frequency to heptanal. Error bars indicate SEM in this and the following figures.

(F) Mean and individual EC_{50} values of different I7 OSNs to heptanal and octanal. ***$p < 0.001$ (between-group t test).

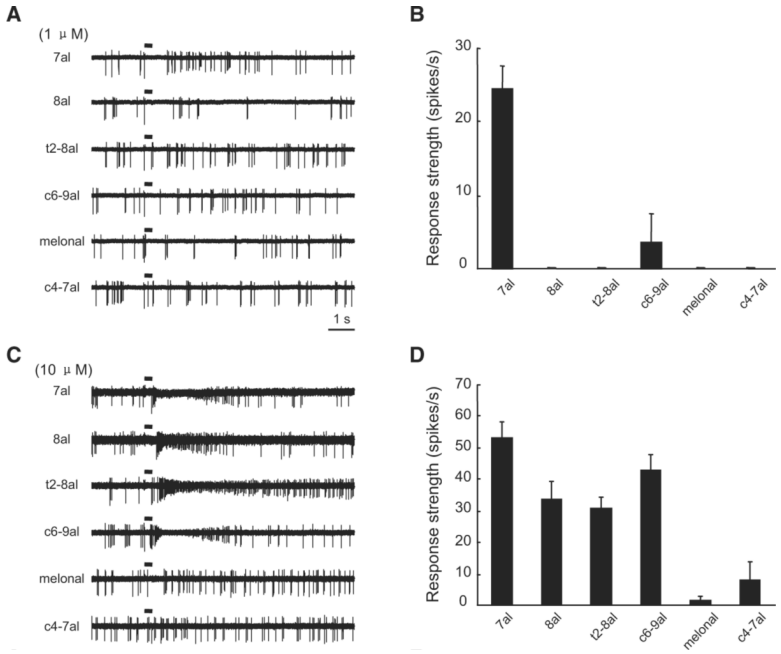

Figure 2. I7 OSNs Respond Selectively to Heptanal at a Low Concentration, but Are Activated by Several Other Aldehydes at a Higher Concentration

(A) Traces showing the responses of a single I7 OSN to six different aldehydes at 1 μM. In this and the following figures, odorants are abbreviated as follows: trans-2-octenal, t2-8al; cis-6-nonenal, c6-9al; 2,6-dimethyl-5-heptenal, melonal; cis-4-heptenal, c4-7al.

(B) Mean response strengths of I7 OSNs to the six aldehydes at 1 μM (n = 5 cells).

(C) Traces showing responses of another I7 OSN to the same set of odorants as in (A) but at 10 μM.

(D) Mean response strengths of I7 OSNs to the six aldehydes at 10 μM (n = 5 cells).

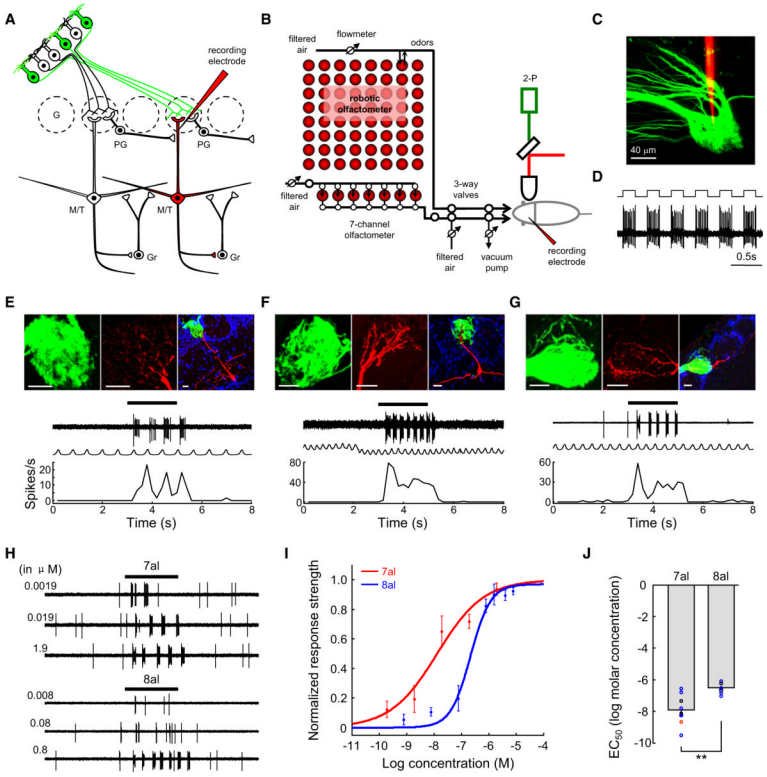

Figure 3. I7 M/T Cells Respond Sensitively to Heptanal, whereas Sensitivity to Octanal Is Significantly Lower

(A) Schematic representation of simplified circuitry in the MOB and our experimental strategy. A dye- and neurobiotin-filled glass electrode (red pipette) was targeted to a GFP$^+$ I7 glomerulus to search for I7 M/T cells. Their firing of action potentials was extracellularly recorded, likely from the primary dendritic trunks of M/T cells. The recorded neurons were then juxtacellularly labeled (red), and their relationship with the I7 glomerulus was confirmed by the presence of dye-filled primary dendritic tufts exclusively in GFP$^+$ glomerulus. G, glomerulus; Gr, granule cells. In this and the following figures, short axon cells are not shown for simplicity.

(B) Schematic representation of the experimental setup. GFP$^+$ glomeruli were visualized by two-photon microscopic imaging. Odorants were stored in headspace vials on an 8 × 8 panel and delivered with a custom-made robotic olfactometer. Two headspace vials in the panel containing pure air or air with mineral oil were used as controls. An additional set of seven aldehydes was delivered by a custom-made seven-channel olfactometer.

(C) A two-photon microscopic image shows the targeting of tetramethylrhodamine dextran amine-filled recording pipette (red) into the I7 glomerulus (green).

(D) During juxtacellular labeling, the firing of the recorded cell was tightly synchronized with current injection.

(E–G) Three examples showing heptanal-evoked responses from different subtypes of I7 M/T cells (a mitral cell in E, a middle tufted cell in F, and an external tufted cell in G). (Top panels) Juxtacellular labeling revealed that the recorded cells (red) extended their primary dendritic tufts into dorsal I7 glomeruli labeled with GFP (green). Blue, DAPI labeling to delineate glomeruli. Below the images are physiological traces, respiratory rhythms, and mean peristimulus time histogram (PSTH) plots showing that heptanal evoked strong firing of action potentials from these cells. In all three examples, heptanal was diluted as 1% saturated vapor. In this and the following figures, horizontal bars above physiological traces represent 2 s odorant pulses and serve as timescale as well. Scale bars, 20 µm.

(H) Physiological traces showing the response intensities of a mitral cell to heptanal and octanal at different concentrations. The concentrations shown on the left (in μM) were calculated from the dilutions of saturated vapor pressure of heptanal and octanal. For heptanal, 1% dilution of saturated vapor corresponds to 1.9 μM.
(I) Dose-response curves of I7 M/T cells to heptanal (n = 8 cells) and octanal (n = 7 cells). The response strengths were normalized to the saturated response strength of I7 M/T cells to heptanal.
(J) Mean EC_{50} values of I7 M/T cells to heptanal were significantly lower than those to octanal (**$p < 0.01$; t test). The colors of circles code for different cell subtypes in this figure and Figure 4D. Red, mitral cells; blue, middle tufted cells; black, external tufted cells.
See also Figure S1 and Table S1.

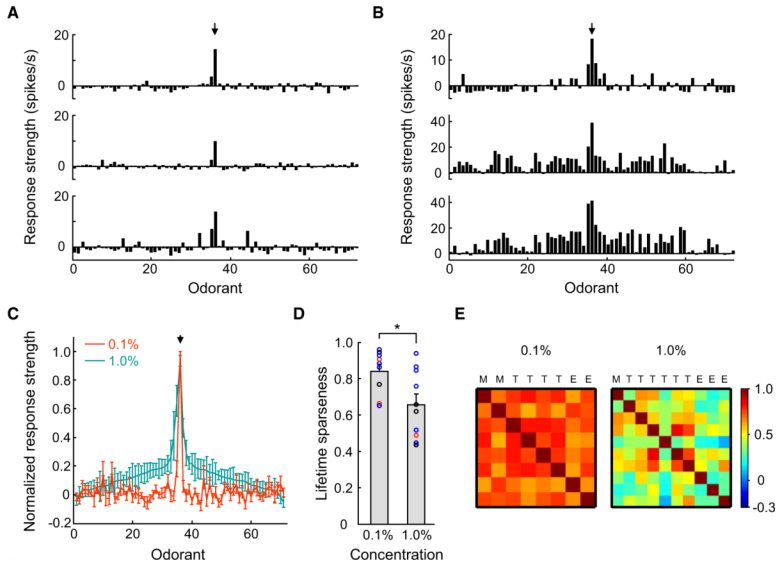

Figure 4. I7 M/T Cells Exhibit Sharp Tuning Curves, with Heptanal Being the Most Effective Stimulus

(A) Tuning curves of three I7 M/T cells in response to a diverse set of odorants, all at 0.1% dilutions of saturated vapor. Mean response strength to each odorant is plotted against odorant identity (Table S2). Arrow points to the strength of response to heptanal.

(B) Tuning curves of three additional I7 M/T cells in response to the same set of odorants at 1% dilution.

(C) Comparison of the mean tuning curves of I7 M/T cells at 0.1% and 1% dilutions (n = 9 and 10 cells, respectively). Response intensities were normalized to the maximum responses of the cells to heptanal. Odorant identities are aligned to produce a smooth tuning curve for responses to odorants at 1% dilution, with a maximum response in the middle. The alignment of odorant identities is identical for horizontal axes in (A)–(C) and is listed in Table S2.

(D) The lifetime sparseness (S) value of I7 M/T cells to odorants at 0.1% dilution is significantly higher than that at 1% (*$p < 0.05$; t test between concentrations). Circles indicate S values of individual M/T cells.

(E) The matrices of Pearson's correlation coefficients for the tuning curves across individual I7 M/T cells at concentrations of 0.1% (left-hand panel, mean coefficient = 0.72 ± 0.06, mean ± STD) and 1% (right-hand panel, 0.44 ± 0.016). Color bar indicates the range of correlation coefficients. M, mitral cells; T, middle tufted cells; E, external tufted cells.

See also Figure S2 and Table S2.

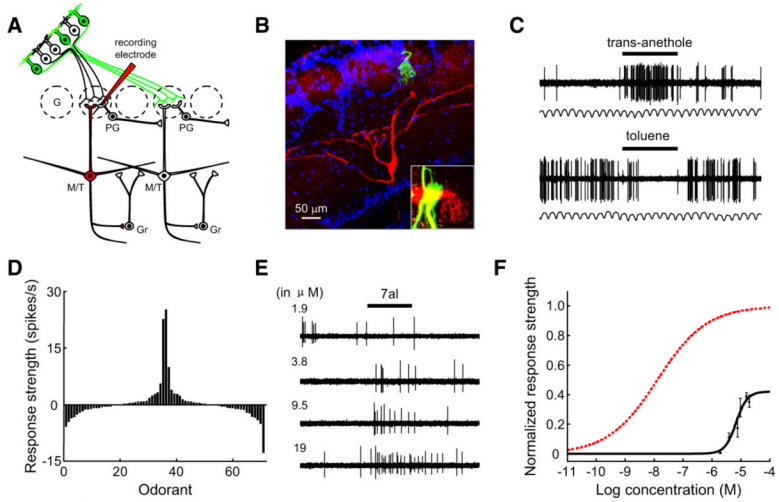

Figure 5. Near-I7 M/T Cells Are Narrowly Tuned and Lack Responses to Heptanal

(A) Schematic representation of recording strategy. M/T cells associated with glomeruli adjacent to the GFP$^+$ I7 glomerulus were recorded and labeled.

(B) The morphology of a mitral cell (red) that extended its primary dendrite into a glomerulus adjacent to the dorsal I7 glomerulus (green). Blue, DAPI staining. Inset shows the dorsal view of the dye-filled dendritic tufts and electrode (red) near the green I7 glomerulus. The image in the inset was collected in vivo immediately after recording.

(C) Firing patterns of the cell in (B) showing representative excitatory (upper trace) and inhibitory (lower trace) responses to odorant at 1% dilution.

(D) Tuning curve of the cell shown in (B) in response to 69 different odorants at 1% dilution.

(E) Physiological traces showing the response intensities of a near-I7 mitral cell to heptanal at different concentrations.

(F) Dose-response plot and fitted sigmoid function of four near-I7 M/T cells (black) that were activated by heptanal. The red dashed curve indicates the mean dose-response plot of I7 M/T cells for heptanal.

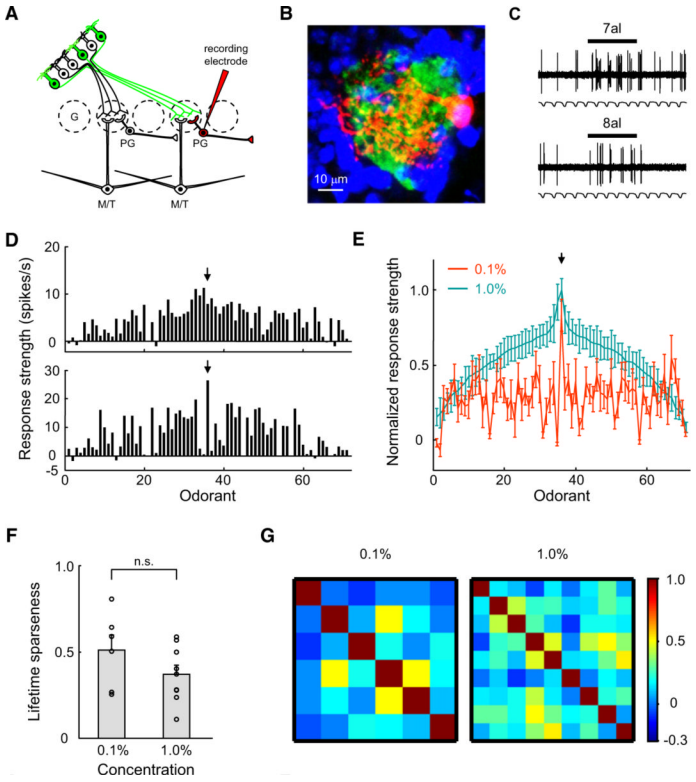

Figure 6. I7 PG Cells Respond Broadly and Heterogeneously

(A) Schematic representation of experimental strategy for recording I7 PG cells.

(B) Juxtacellular labeling revealed that a PG cell (red) extended its dendrites exclusively into an I7 glomerulus (green). Blue, DAPI staining.

(C) Physiological traces of the cell in (B) showing representative excitatory responses to 2 s pulses of heptanal and octanal at 1% dilution.

(D) Two examples of tuning curves of I7 PG cells to 69 odorants at 1%. Arrows point to the strengths of responses to heptanal.

(E) Comparison of the mean tuning curves of I7 PG cells at the concentrations of 0.1% (n = 6 cells) and 1% (n = 9 cells). Odorant identities are aligned so that the mean tuning curve at high concentration is smooth, with maximum response in the middle. The odorant identities in horizontal axes of (D and E) are identical and are listed in Table S2.

(F) The lifetime sparseness values of I7 PG cells at 0.1% and 1%.

(G) The matrices of Pearson's correlation coefficients for the tuning curves across individual I7 PG cells at the concentrations of 0.1% (left-hand panel, mean coefficient = 0.13 ± 0.18) and 1% (right-hand panel, 0.20 ± 0.15).

See also Figure S3 and Table S2.

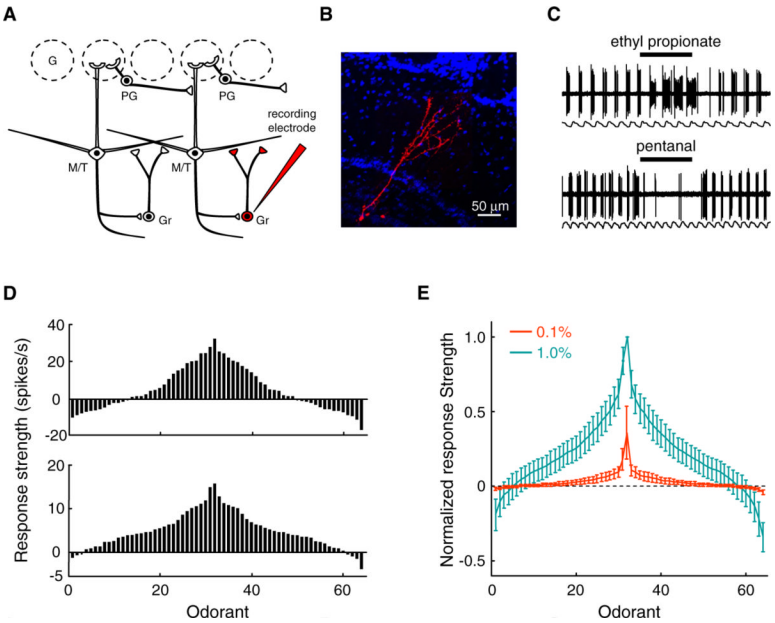

Figure 7. Granule Cells in the MOB Are Broadly Tuned

(A) Schematic representation of recording strategy. Granule cells were randomly recorded and labeled by lowering electrodes into the granule cell layer.

(B) The morphology of a granule cell, which belongs to the most abundant neuron type in the bulb.

(C) The granule cell in (B) shows both excitatory and inhibitory responses to odorants at 1% dilution.

(D) Two examples of tuning curves of granule cells to 64 odorants at 1% dilution. (Upper panel) The tuning curve of the granule cell shown in (B) at 1% dilution. (Lower panel) The tuning curve of another granule cell illustrating the lack of inhibition.

(E) Mean tuning curves of granule cells to 64 odorants at 0.1% and 1% dilutions (n = 5 and 8 cells, respectively). The response strengths of granule cells to odorants at 0.1% dilutions are normalized to the mean peak responses of granule cells to odorants at 1% dilutions.

See also Figure S4.

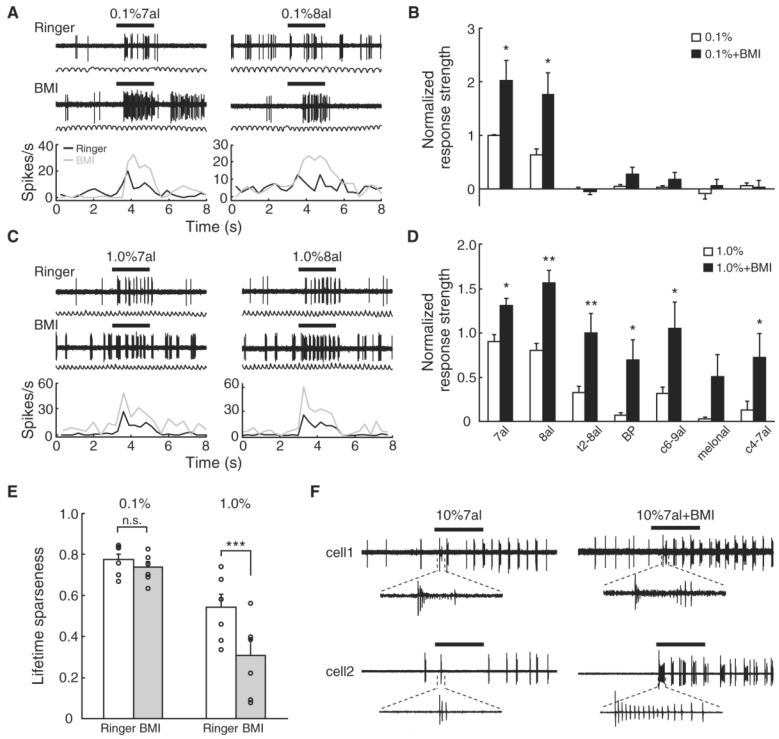

Figure 8. Inhibitory Connections in the MOB Enhance Response Selectivity of I7 M/T Cells to Odorants at High Concentrations

(A) Traces (upper panel) and PSTHs (lower panel) of an I7 M/T cell to 0.1% heptanal and octanal before (black lines) and after (gray lines) bicuculline methiodide (BMI, 200 mM) superfusion.

(B) The effects of BMI application on the response strengths of I7 M/T cells to seven odorants at 0.1% dilution (n = 6 cells). Response strengths were normalized to the responses evoked by the most effective odorant before BMI application. BP, butyl propionate; other odorants were abbreviated using conventions in Figures 1 and 2. *$p < 0.05$ (paired t test between responses before and after BMI).

(C) Traces and PSTHs of another I7 M/T cell to 1% heptanal and octanal before and after BMI application.

(D) The effects of BMI application on the response strength of I7 M/T cells to seven odorants at 1% dilution (n = 6 cells). *$p < 0.05$; **$p < 0.01$ (paired t test between responses before and after BMI).

(E) BMI application reduced the lifetime sparseness (S) values of I7 M/T cells in response to odorants at 1% dilution but not 0.1% dilution. n.s., not significant; ***$p < 0.001$ (paired t test between responses before and after BMI). The overall S values here were lower than those when tested with 69 odorants because only a small subset of aldehydes were used, resulting in a biased stimulus set.

(F) Examples showing the response patterns of two I7 M/T cells to 10% heptanal before (left panel) and after (right panel) BMI application.

See also Figure S5.